INSTRUMENTATION

Investigation of Contribution Functions in a Scintillation Camera

Ken Ueda, Fumio Kawaguchi, Katsumi Takami, and Kenji Ishimatsu

Hitachi Central Research Laboratory, Hitachi Ltd., and Hitachi Medical Corporation, Tokyo, Japan

The statistical spatial resolution and coordinate linearity at the central portion of an image detector are investigated theoretically in relation to the "contributing factor of a photomultiplier (PM) to a positioning signal" and light-guide thickness. The "contributing factor" is the increment of change in the positioning signal corresponding to an infinitessimal change in PM output. The "contribution function to a positioning signal" of a PM group with equal x or y coordinates is defined by this "contributing factor" and expressed as a function of the relative position between the PM group and a scintillation point. When the "contribution function" is determined, the statistical spatial resolution and coordinate linearity can be calculated for a given light-guide thickness.

The ideal contribution functions, which are two-dimensional, minimize the resolving distance when light-guide thickness is in the range of 0.6–0.7 times the PM radius. The contribution functions of the matrix and threshold-preamplifier methods, which are approximately one-dimensional, cannot correct the coordinate nonlinearity, which increases as light-guide thickness decreases, although the threshold-preamplifier method improves resolving distance. Modification of the one-dimensional contribution functions—which reduce the nonlinearity to one half or less accompanied by only a slight increase in resolving distance—are proposed. If the acceptable nonlinearity is ±4%, the resolving distance decreases by 26 and 14% over the matrix and threshold-preamplifier methods, respectively, by using the modification for thin light guides.

J Nucl Med 19: 825–835, 1978

The scintillation camera developed by Anger (*1–3*) has been used widely to image the distribution of radionuclides in vivo. Some theoretical studies (*4–11*) have been made to improve the intrinsic spatial resolution and reduce the edge effect. The average spatial resolution and the average coordinate linearity in an overall field of view are related to light-guide thickness (*9*). This thickness is the perpendicular distance between a scintillation site and the photocathode plane. Linearity in the central portion of an image, however, cannot be estimated accurately from the averaged linearity, because the latter is mainly affected by the edge effect (*10*). Investigations of linearity and spatial resolution at the central region of an image appear not to have been made to date.

Tanaka et al. (*11*) investigated position-computing arithmetics. They defined the "contributing factor" of a photomultiplier (PM) to a positioning signal as the increment of change in the positioning signal corresponding to an infinitely small change in the output of the PM. When the contributing factors of all PMs are given for any scintillation point, spatial resolution and coordinate linearity are calculated for a given light-distribution model. They have expressed mathematically the optimum set of the contributing factors that attain both the theoretical

Received June 28, 1977; revision accepted Nov. 30, 1977.

For reprints contact: Ken Ueda, Hitachi Central Research Laboratory, Hitachi Ltd., 1-280, Higashikoigakubo, Kokubunji-shi, Tokyo, 185, Japan.

minimum resolving distance and perfect coordinate linearity for a given light distribution. A position-computation method based on delay-line time conversion (*11–14*) has been developed, and some improvements in spatial resolution and linearity have been achieved by experimental optimization of the contributing factors. An improvement in spatial resolution using threshold preamplifiers (*15*) is also considered a modification of the contributing factors.

Experimental work has been carried out using the delay-line position-computing method. As a result, a large-area, high-resolution scintillation camera has been developed (*16–20*), which visualizes a 2.0 mm bar phantom using Co-57 (122 keV) gamma photons in a field 330 mm in diameter. First, however, this required the investigation of the contributing factors. In the present work, the spatial resolution and coordinate linearity for the central portion of the image detector are discussed in terms of the contributing factors and light distribution.

A diagram of the optical systems under consideration is depicted in Fig. 1, where the radius of all PMs is normalized to 1. The range of scintillation-point coordinates is limited to $0 \leqq x_o \leqq 1$ and $0 \leqq y_o \leqq \sqrt{3}$, so that performances are not affected by the edge effect that results from the limited array of PMs.

A simple assumption is applied with regard to light distribution, which is that the mean output of a PM is proportional to the solid angle subtended at the scintillation point by the photocathode (*21*). Refraction and scatter of scintillation light at interfaces is not taken into account. This simple model is one that has been widely applied (*4,9*). Furthermore, the main purpose of the work is to compare different position-computing arithmetics and to make a general investigation of linearity correction, since this is the first time an investigation of "contribution function" (defined below) has been conducted.

An applied model of position computation is as follows. When a positioning signal for the x direction is to be calculated, the output of PMs with equal x coordinates is first summed. The PM group in a line is termed the x-coordinate line, and the sum of their outputs is termed the x-coordinate-line signal. Then the x-coordinate-line signal, expressed as a function of relative positions of an x-coordinate line and a scintillation point, is termed the "line-signal function." In the same manner, the "contributing factor" to the positioning signal of an x-coordinate line, expressed as a function of the same relative positions, is termed the "contribution function."

First we will show that when the "contribution function" is determined, statistical spatial resolution and coordinate linearity can be calculated for a given "line-signal function." Next, the ideal contribution function and the theoretical minimum resolving distance are discussed. Then performances obtained by the conventional position computations of the matrix and threshold-preamplifier methods are compared. Finally, modifications of one-dimensional contribution functions, which reduce the nonlinearity, are considered and the resulting performances are discussed.

Ideal contribution function for position computation. A position signal, X, obtained by position computation, is a function of PM outputs $[z_j\ (j = 1, \ldots, N)]$, where z_j is a function of the position coordinates (x_o,y_o) for the scintillation point. $X = X[z_j(x_o,y_o), j = 1, \ldots N]$. The number of photoelectrons, n_j, reaching the first dynode of the j-th PM is assumed to fluctuate according to the Poisson distribution law. Signals from different PM tubes are assumed not to influence each other. The gains, G, of all PMs are assumed to be equal. Therefore the standard deviation σ_x of the X is given by

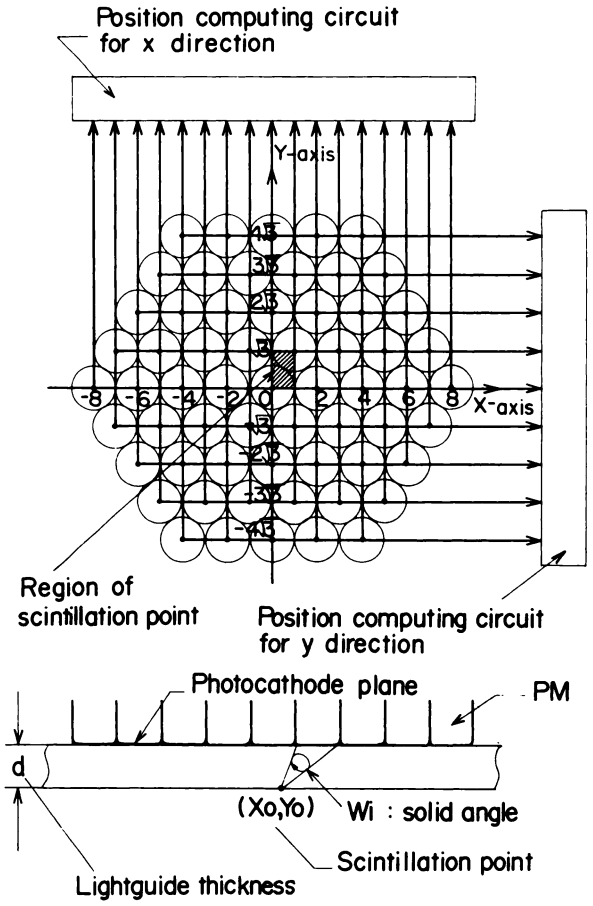

FIG. 1. Diagram of PM array for a 61-tube system.

$$\sigma_x(x_o,y_o) = \left[\sum_j \left(\frac{\partial X}{\partial z_j} \cdot \sigma_{zj}\right)^2\right]^{1/2} = G\left(\sum_j k_j^2 \cdot n_j\right)^{1/2}, \quad (1)$$

in which $\sigma_{zj}(= G\sqrt{n_j})$ is the standard deviation of z_j, and $k_j(= \partial X/\partial z_j)$ is the "contributing factor" of the j-th PM to the position signal.

The calculation of the positioning signal in the x direction is considered. The relative position (u,v) between an x-coordinate line, where the x coordinate is x_m, and a scintillation point (x_o,y_o) is

$$u = x_m - x_o, \quad (2)$$

$$v = \begin{cases} y_o & \text{for even } x_m, \\ \sqrt{3} - y_o & \text{for odd } x_m, \end{cases} \quad (3)$$

where v represents the absolute of the difference between y_o coordinate of the PM that is nearest the scintillation point on the x-coordinate line. It is suggested that when $0 \leqq y_o \leqq \sqrt{3}$ (see Fig. 1), the y coordinate of this PM is 0 for an even value of x_m, and $\sqrt{3}$ for an odd value.

When the line-signal function is denoted by $Z_x(u,v)$, $N_x(u,v)$ in the following formula is the sum of photoelectrons reaching the first dynode of PMs with equal x coordinates:

$$N_x(u,v) = \frac{1}{G} \cdot Z_x(u,v). \quad (4)$$

The contribution function $K_x(u,v)$ is then defined as

$$K_x(u,v) = \frac{\partial X}{\partial Z_x}. \quad (5)$$

Therefore Eq. 1 can be rewritten as

$$\sigma_x(x_o,y_o) = G\left(\sum K_x^2 \cdot N_x\right)^{1/2}. \quad (6)$$

The summation in Eq. 6 is made for all x_m values, that is, $-8, -7, \ldots, +7, +8$, for the model in Fig. 1. Position sensitivity $S_x(x_o,y_o)$ is expressed as

$$S_x(x_o,y_o) = \frac{\partial X}{\partial x_o} = -G \cdot \sum K_x \frac{\partial N_x}{\partial u}. \quad (7)$$

Position sensitivity, expressed as a function of the coordinates of scintillation points, is equivalent to coordinate linearity. Accordingly, the statistical resolving distance—in terms of standard deviation, normalized by the position sensitivity—is expressed as

$$R_x(x_o,y_o) = \frac{\sigma_x}{S_x} = \frac{\left(\sum K_x^2 N_x\right)^{1/2}}{-\sum K_x \frac{\partial N_x}{\partial u}}. \quad (8)$$

It follows that both coordinate linearity and statistical resolving distance are determined by the combination of the line signal and contribution functions. The ideal contribution function, $K_{xi}(u,v)$, for the line-signal function, $Z_x(u,v)$, is defined so that R_x is minimized and S_x is constant for any (x_o,y_o). It is expressed (*11*) as

$$K_{xi}(u,v) = \frac{-\frac{c}{N_x} \cdot \frac{\partial N_x}{\partial u}}{\sum \frac{1}{N_x} \cdot \left(\frac{\partial N_x}{\partial u}\right)^2}, \quad (9)$$

where c is a positive constant. The theoretical minimum resolving distance R_{xi} obtained by K_{xi} is expressed (*11*) as

$$R_{xi}(x_o,y_o) = \left(\sum \frac{\left(-\frac{\partial N_x}{\partial u}\right)^2}{N_x}\right)^{-1/2}. \quad (10)$$

Note that the theoretical minimum resolving distance is, in general, a function of the scintillation point's coordinates.

Calculation of the y-direction position signal proceeds in the same manner as for the x direction. That is, the line-signal function for the y direction, $Z_y(u,v)$, and the contribution function, $K_y(u,v)$, are defined for the parameters, u, v, in Eqs. 11 and 12:

$$u = \begin{cases} x_o, \text{ for even } y_m, \\ 1 - x_o, \text{ for odd } y_m, \end{cases} \quad (11)$$

$$v = y_m - y_o. \quad (12)$$

The mean PM outputs are computed for a given light-guide thickness by the method developed by Masket et al. (*22*), on the assumption that the mean PM outputs are proportional to the corresponding solid angles. The range of the light-guide thickness, d, under consideration is $0.2 \leqq d \leqq 2.0$. Line-signal and ideal contribution functions for the x and y directions are obtained for a given light-guide thickness, and typical results are shown in Figs. 2 and 3, respectively.

The vibration in the ideal contribution functions in Fig. 3 is attributed to the denominator in Eq. 10, since the denominator, which is equal to $1/R_{xi}^2$, varies slowly. If the contribution function for the x direction has the form

$$K_x(u,v) = -\frac{c}{N_x} \cdot \frac{\partial N_x}{\partial u}, \quad (13)$$

the theoretical minimum spatial resolution may be obtained, but the corresponding position sensitivity (S_x) varies. This indicates a loss of coordinate linearity. As light-guide thickness decreases, the vibration amplitude in the denominator in Eq. 10 increases. Therefore, radical changes in the form of the contribution function are required to adjust for a slight change in the coordinates of scintillation points.

The theoretical minimum resolving distances, R_{xi} and R_{yi}, given by Eq. 10 for various values of the

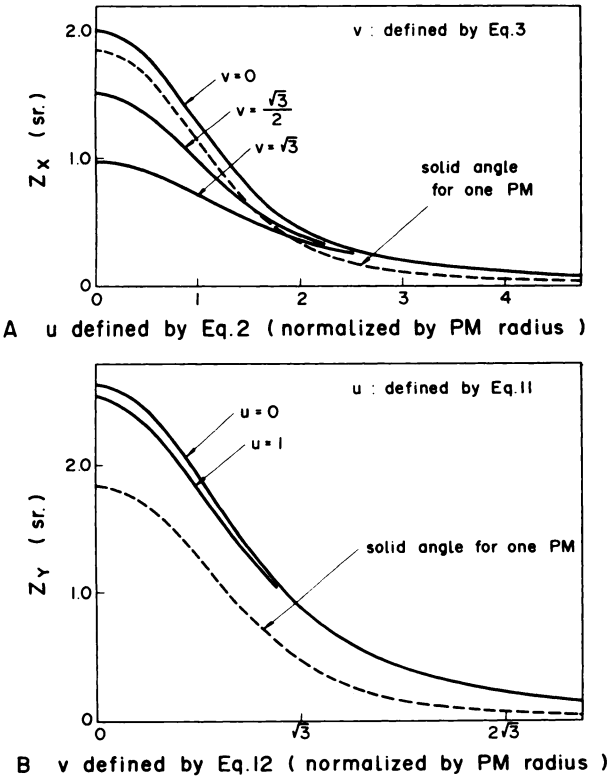

FIG. 2. Line-signal functions for d = 1.0 in first quadrant for x (A) and y (B) directions. Broken lines show solid angle for one PM as function of distance between PM and scintillation point. Waveforms are symmetric with respect to longitudinal axis. Values of line-signal functions are only weakly related to number of PMs with equal x or y coordinates (N_p) in Fig. 1. Here, N_p is taken as $\neq 5$ and 7 for x and y directions, respectively.

light-guide thickness, d, are plotted in Fig. 4. Note that R_{xi} is maximum at (0,0) and minimum at (1,0), whereas R_{yi} is also maximum at (0,0), but its minimum is near (0, $\sqrt{3}/2$). The difference between R_{xi} (0,0) and R_{yi} (0,0 for a given d value is within 1%. These values are minimized when d is in the 0.6–0.7 region (Fig. 5).

Both the ideal contribution functions and the theoretical minimum resolving distance are determined only by the light-distribution characteristics. They therefore represent determinant features of optical systems.

Position computation by the matrix method. In a signal-matrix circuit, which is the conventional position computer of Anger cameras, the position signal X is given (*9,10,12*) by

$$X(x_o,y_o) = \frac{\sum x_m \cdot Z_x}{\sum Z_x} = \frac{\sum x_m \cdot N_x}{\sum N_x}, \quad (14)$$

where the gains of all PMs are assumed equal. The contribution function by a matrix circuit is derived from Eqs. 3, 4, and 5 as

$$K_x(u,v) = \frac{u\left(1 + \frac{x_o - X}{u}\right)}{G \cdot \sum N_x}. \quad (15)$$

For a well-designed scintillation camera of the matrix type, K_x is nearly proportional to u and nearly independent of v, because $\sum N_x \simeq$ constant and $(x_o - X)/u \simeq 0$ in the central portion of the image. The position sensitivity and resolving distance are derived from Eqs. 8, 9, and 15 as follows:

$$S_x(x_o,y_o) = \frac{-\sum u \cdot \left(1 + \frac{x_o - X}{u}\right) \cdot \frac{\partial N_x}{\partial u}}{\sum N_x}. \quad (16)$$

$$R_x(x_o,y_o) = \frac{\{\sum u^2 \cdot \left(1 + \frac{x_o - X}{u}\right)^2 \cdot N_x\}^{1/2}}{-\sum u\left(1 + \frac{x_o - X}{u}\right) \cdot \frac{\partial N_x}{\partial u}}. \quad (17)$$

The coordinate nonlinearity in the x direction is taken as

$$L_x = \frac{\max(S_x) - \min(S_x)}{\max(S_x) + \min(S_x)} \cdot 100\,(\%), \quad (18)$$

where $\max(S_x)$ and $\min(S_x)$ are the maximum and minimum S_x values for a given light-guide thickness. The same treatment is applied to the y-direction position signal. The values of S_x, S_y, R_x, and R_o were calculated in the range of $0 \leqq x_o \leqq 1$ and $0 \leqq y \leqq \sqrt{3}$ for $0.2 \leqq d \leqq 2.0$.

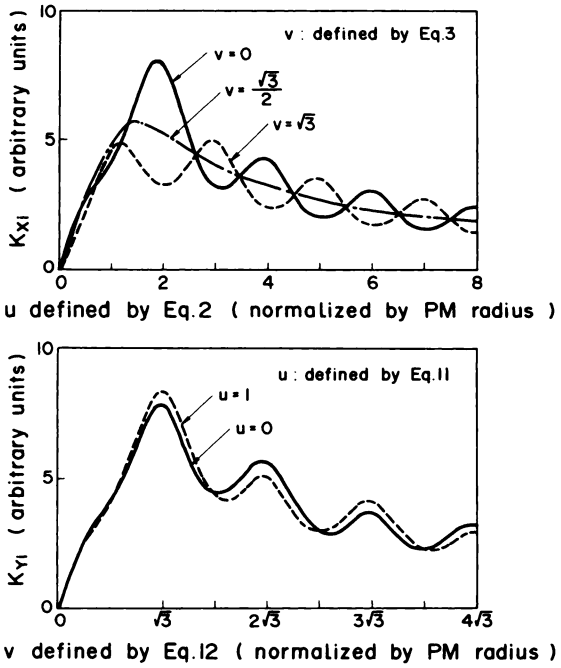

FIG. 3. Ideal contribution functions for d = 1.0 in first quadrant for x (A) and y (B) directions. Waveforms are symmetric with (0,0). Ideal contribution values are only weakly related to N_p. Here, N_p = 5 and 7 for x and y directions, respectively.

Dependence of the resolving distance on scintillation position is similar to that of the theoretical minimum. The dependence of the resolving distance and position sensitivity turns out to be the reverse. That is, R_x and R_y are maximum and S_x, S_y minimum at (0,0). R_x will be minimum and S_x maximum at (1,0); R_y is minimum and S_y maximum near (0, $\sqrt{3}/2$). The values, max(R_x), max(R_y), L_x, and L_y are shown as a function of d in Fig. 5. The nonlinearity inherent in this position computation increases rapidly as light-guide thickness decreases, and is discussed later.

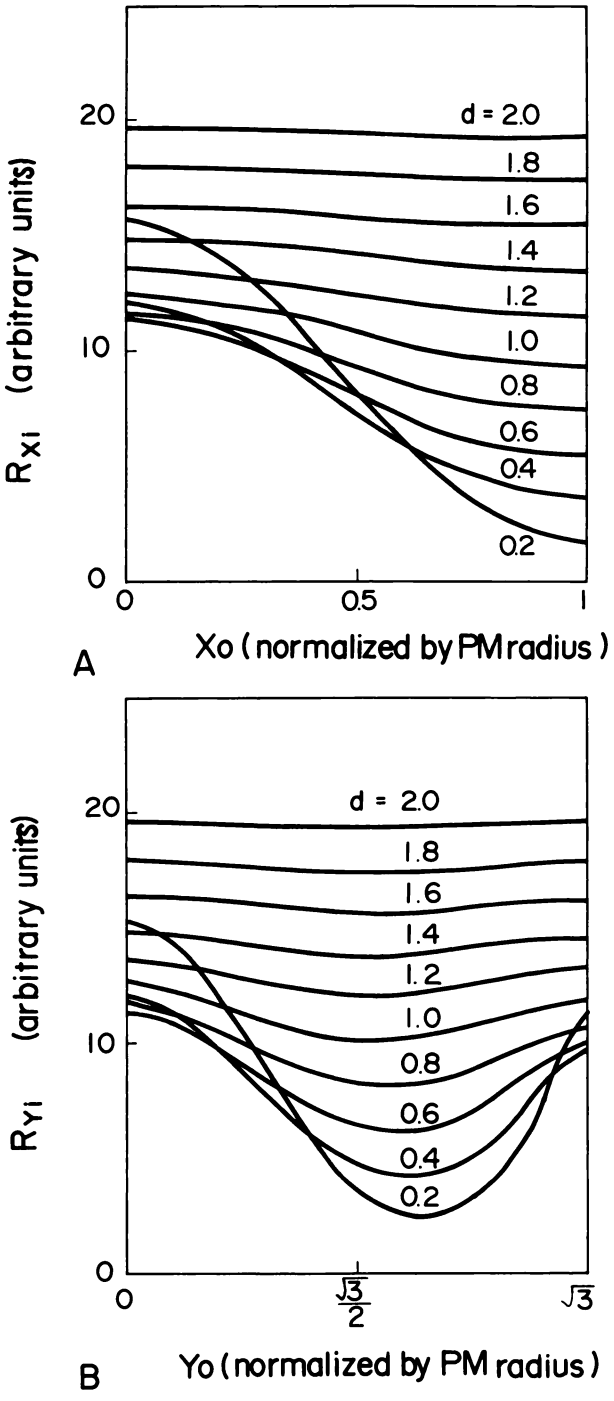

FIG. 4. Theoretical minimum resolving distance for x direction (A) where $y_o = 0$, and y direction (B) where $x_o = 0$.

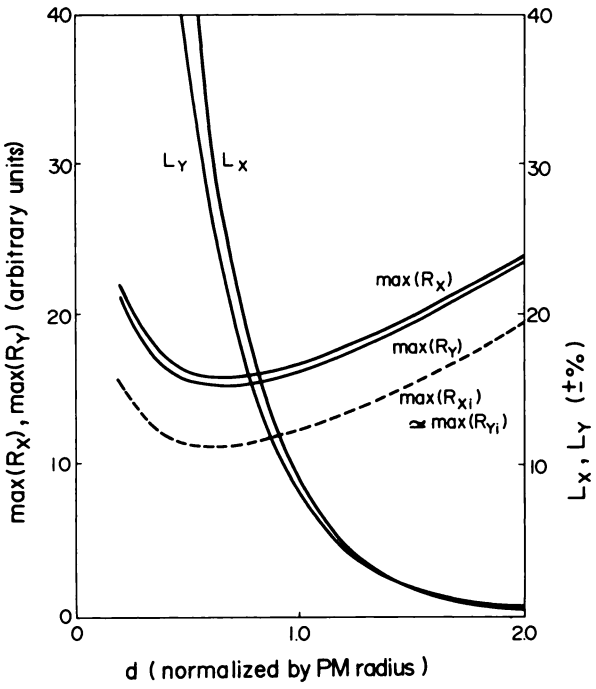

FIG. 5. Resolving distance and nonlinearity for matrix method.

Threshold-preamplifier method. If a set of nonlinear preamplifiers is adopted for each x-coordinate line signal before a signal-matrix circuit, Eqs. 19 and 20 hold true instead of Eqs. 14 and 15, respectively:

$$X = \frac{\sum x_m \cdot g(z_j)}{\sum g(z_j)} \tag{19}$$

$$K_x(u,v) = \frac{\frac{dg}{dZ_x}(z_j) \cdot u \cdot \left(1 + \frac{x_o - X}{u}\right)}{\sum g(z_j)}, \tag{20}$$

where $g(z_j)$ is the output of a nonlinear preamplifier for an input signal z_j. The contribution function for this circuit is derived as

$$K_x(u,v) = \begin{cases} \dfrac{u\left(1 + \dfrac{x_o - X}{u}\right)}{\sum (Z_x - T)}, & \text{for } Z_x \geqq T, \\ 0, \text{ for } Z_x < T, \end{cases} \tag{21}$$

where T is the threshold level for each x-coordinate line signal.

A contribution function, in a pyramidal form presented by Eq. 22, is assumed here as a simplified model for the threshold-preamplifier method, because a characteristic threshold-preamplifier curve generally has a tail below the threshold level (*23*):

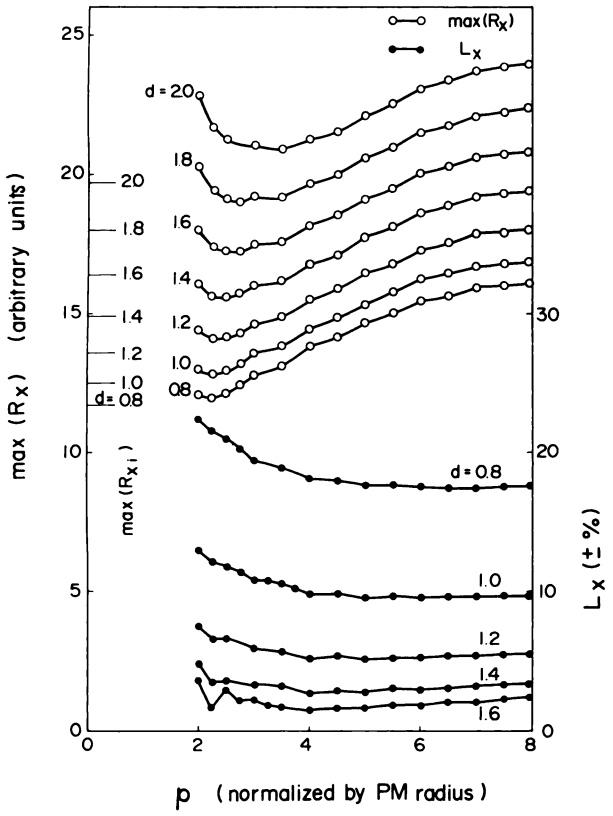

FIG. 6. Resolving distance and nonlinearity for x direction by pyramidal contribution functions, which are simplified models of threshold-preamplifier method.

$$K_x(u,v) = \begin{cases} u, \text{ for } |u| \leqq p, \\ 2p - u, \text{ for } p \leqq u \leqq 2p, \\ -2p - u, \text{ for } -2p \leqq u \leqq -p, \\ 0, \text{ for } |u| \geqq 2p. \end{cases} \quad (22)$$

The p value where K_x is maximum is related to T as $Z_x(p,v) \simeq T$.

The resolving distance and nonlinearity were calculated, for various d and p values, from Eqs. 7, 8, 18, and 22. The results are shown in Figs. 6 and 7. These figures suggest that spatial resolution may be improved to approximately that of a small detector employing only 19 PMs, by the reduction in the p values from 8 to 4 for K_x and from $4\sqrt{3}$ to $2\sqrt{3}$ for K_y. Further reduction of p to 2–3 and $\sqrt{3} - 2\sqrt{3}$ regions for the x and y directions may improve the resolving distances to values that are 5% over the theoretical minimum. In these cases, however, some linearity is lost.

Thus, the threshold-preamplifier method is adaptable to thick light guides, which achieve good linearity and may be effective in improving the spatial resolution of large-area detectors. This method, however, cannot make the best use of thin light guides, because it cannot correct the inherent nonlinearity.

One-dimensional contribution functions that improve nonlinearity. First let us consider the correction of the nonlinearity along the x axis (i.e., $y_o = 0$) by adjustment of the one-dimensional contribution function, $K_x(u)$. The nonlinearity over the xy plane is evaluated later. The position sensitivity along the x axis, $S_x(x_o,0)$, can be expressed as

$$S_x(x_o,0) = -\sum K_x \cdot \frac{\partial N_x}{\partial u}. \quad (23)$$

Assume a function, $h_x(u)$, that is defined over $|u| \leqq w$ and is symmetric about the origin. If $h_x(u)$ satisfies the following equations:

$$-\sum(K_x(u) + h_x(u)) \cdot \frac{\partial N_x}{\partial u} = S_{xh} = \text{constant}, \quad (24)$$

$$h_x(0) = h_x(w) = h_x(-w) = 0, \quad (25)$$

$$K_x(u) + h_x(u) \geqq 0, \text{ at } 0 \leqq u \leqq w, \quad (26)$$

where w is a constant, then a contribution function, $K_{xh}(u)$, can be obtained that realizes perfect linearity along the x-axis:

$$K_{xh}(u) = K_x(u) + h_x(u). \quad (27)$$

This function, $K_{xh}(u)$, obtained under conditions where $w = 2$, is investigated here. This is because it

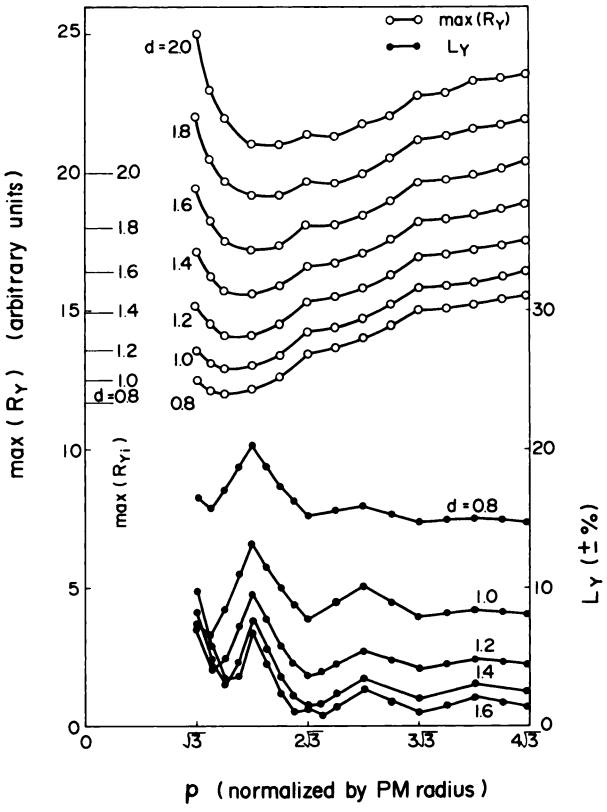

FIG. 7. Resolving distance and nonlinearity for y direction by pyramidal contribution functions, which are simplified models of threshold-preamplifier method.

can be calculated as follows, and approximated by the delay-line position computation (*12*). The value $K_{xh}(1)$ is determined first for a given d value and an initial condition of $K_{xh}(2)$ by

$$K_{xh}(1) = K_x(1) + \frac{S_x(1,0) - S_x(0,0)}{2\left(\frac{\partial N_x}{\partial u}(1,0) - \frac{\partial N_x}{\partial u}(1,\sqrt{3})\right)}. \quad (28)$$

Then, for a given $K_{xh}(u)$ for $1 < u < 2$, $K_{xh}(u)$ values for $0 < u < 1$ are determined, and the whole $K_{xh}(u)$ can be obtained as shown in Fig. 8. Note that $K_{xh}(u)$ for $|u| \leqq 2$ is a function of $K_x(u)$ for $|u| > 2$, as well as $|u| \leqq 2$, since $S_x(1,0)$ and $S_x(0,0)$ in Eq. 28 are functions of $K_x(u)$. The details of the computation are shown in Appendix 1.

A distinctive feature in this figure is that $K_{xh}(1)$ decreases as d decreases. The value C_x is defined here as

$$\frac{K_{xh}(2) - 2K_{xh}(1)}{K_{xh}(2)}, \quad (29)$$

which represents the deviation of $K_{xh}(1)$ from the contribution function obtained by the matrix and threshold-preamplifier methods. Examples of C_x are shown in Fig. 9. The value appears sensitive to the d value but rather insensitive to the p value that determines the original waveform of $K_{xh}(u)$ for $|u| \geqq 2$.

Since nonlinearity depends primarily on $K_x(1)/K_x(2)$ for given values of d and $K_x(u)$ for $|u| \leqq 2$,

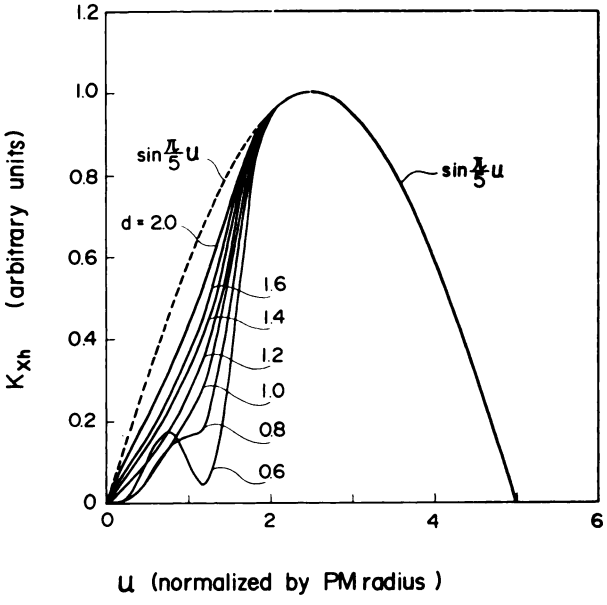

FIG. 8. Examples of corrected one-dimensional contribution functions for x direction. Waveforms are symmetric with (0,0). Functions of K_{xh} are obtained under the condition where $K_x(x) = \sin(\pi x/5)$ for $|x| \leqq 5$, because this condition is approximately realized by delay-line position computation (*12*).

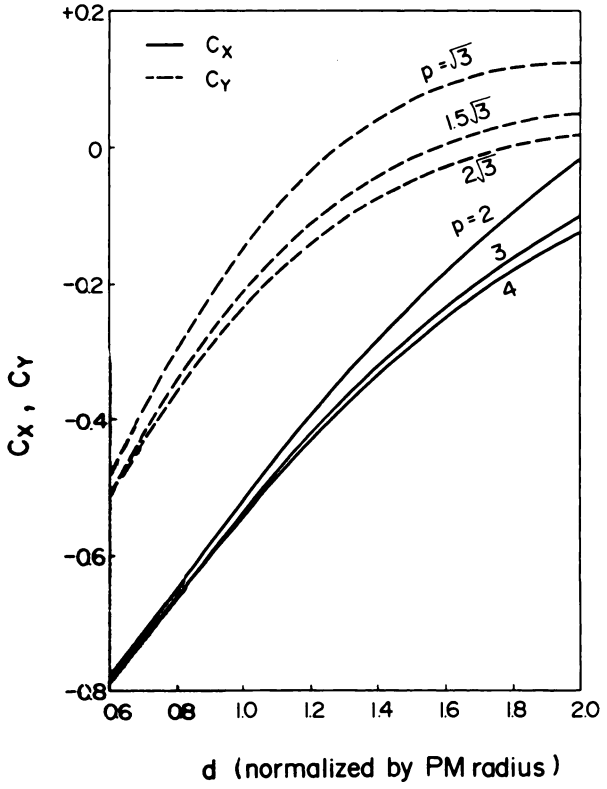

FIG. 9. Values of C_x and C_y, obtained when $K_{xh}(u) = \sin(\pi u/2p)$ for $2 \leqq |u| \leqq 2p$, and $K_{yh}(v) = \sin(\pi v/2p)$ for $3 \leqq |v| \leqq 2p$. Here, p is u or v value at which $K_{xh}(u)$ or $K_{yh}(v)$ is maximum.

a critical adjustment of $K_x(u)$ is required as the differential coefficient defined by Eq. 30 increases:

$$E_x = \frac{\partial L_x}{\partial\left(\frac{K_x(1)}{K_x(2)}\right)}\Bigg|_{S_x(0,0) = S_x(1,0)}. \quad (30)$$

The differential coefficient, E_x, can be given (see Appendix 2) as:

$$E_x = \frac{\partial L_x}{\partial K_x(1)}\Bigg|_{K_x(1) = K_{xh}(1)\cdot K_{xh}(2)} = \frac{K_xh(2)\left\{\frac{\partial N_x}{\partial u}(1,0) - \frac{\partial N_x}{\partial u}(1,\sqrt{3})\right\}^2}{S_x(1,0)\frac{\partial N_x}{\partial u}(1,\sqrt{3}) - S_x(0,0)\frac{\partial N_x}{\partial u}(1,0)}. \quad (31)$$

Examples of E_x are shown in Fig. 10, and will be discussed later.

The contribution function for the y direction, which attains perfect linearity along the y-axis at first, seems obtainable by similar procedures only if $h_y(v)$ is confined to the range of $|v| \leqq 2\sqrt{3}$. It is difficult, however, to attain both perfect linearity and good spatial resolution for the y direction. The difficulty results because the PMs in a y-coordinate line contact one another, and therefore $N_y(u,v)$ and

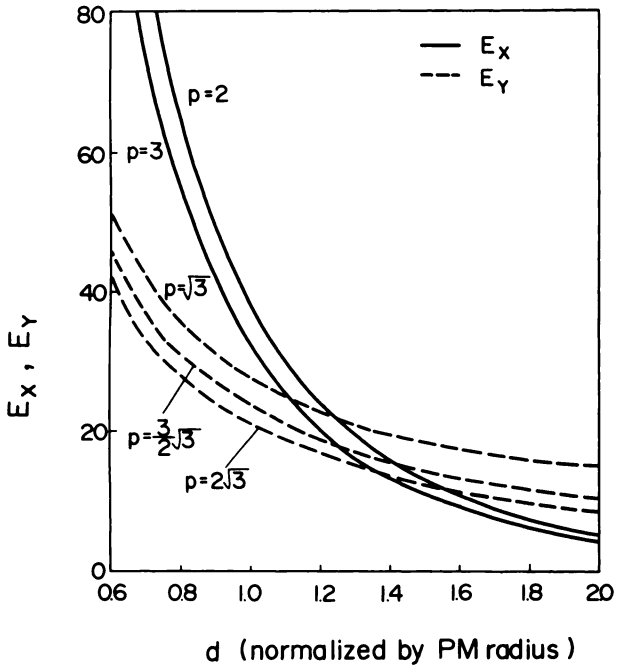

FIG. 10. Values of E_x and E_y, obtained under same conditions as in Fig. 9.

$\partial N_y/\partial v(u,v)$ are almost independent of u (see Fig. 2B). As a result, $S_y(0,0)$ and $S_y(0,\sqrt{3})$ can be written as

$$S_y(0,0) = -2 \cdot K_y(\sqrt{3}) \frac{\partial N_y}{\partial v}(1,\sqrt{3}) - A \quad (32)$$

$$S_y(0,\sqrt{3}) = -2 \cdot K_y(\sqrt{3}) \frac{\partial N_y}{\partial v}(0,\sqrt{3}) - B, \quad (33)$$

where A and B values are nearly equal. In order to attain $S_y(0,0) = S_y(0,\sqrt{3})$, one must maintain $K_y(\sqrt{3})$ at approximately zero, which may cause a considerable loss of spatial resolution. It should be accepted, therefore, that the following inequality remains uncorrected when y_o is near zero:

$$S_y(0,y_o) < S_y(0,\sqrt{3} - y_o). \quad (34)$$

In this paper, correction of $K_y(v)$ to obtain improved linearity is instead considered in the range of $|v| \leqq \sqrt{3}$, because it is possible to adjust most $S_y(0,y_o)$ values to within the range of

$$S_y(0,0) < S_y(0,y_o) < S_y(0,\sqrt{3}). \quad (35)$$

It appears fairly effective in practice, because the difference between $S_y(0,\sqrt{3})$ and $S_y(0,0)$, by the matrix method is, in most cases, considerably smaller than that between $S_y(0,0)$ and $S_y(0,\sqrt{3}/2)$.

In this method, the value of $K_{yh}(\sqrt{3}/2)$ that makes $S_y(0,0) = S_y(0,\sqrt{3}/2)$ can be determined as follows (see Appendix 3):

$$K_{yh}(\sqrt{3}/2) = K_y(\sqrt{3}/2) + \frac{S_y(0,\sqrt{3}/2) - S_y(0,0)}{\frac{\partial N_y}{\partial v}(0,\sqrt{3}/2) + \frac{\partial N_y}{\partial v}A1,\sqrt{3}/2)}. \quad (36)$$

The values C_y and E_y should be defined as follows (see Appendix 3):

$$C_y = \frac{K_{yh}(\sqrt{3}) - 2 \cdot K_{yh}(\sqrt{3}/2)}{K_{yh}(\sqrt{3})} \quad (37)$$

$$E_y = \frac{\partial L_y}{\partial K_y(\sqrt{3}/2)} \Big|_{K_y(\sqrt{3}/2) = K_{yh}(\sqrt{3}/2)} \cdot K_{yh}(\sqrt{3}) = \frac{K_{yh}(\sqrt{3}) \frac{\partial N_y}{\partial v}(0,\sqrt{3}/2) + \frac{\partial N_y}{\partial v}(1,\sqrt{3}/2)}{-4 \cdot S_y(0,0)}. \quad (38)$$

Examples of C_y and E_y are shown in Figs. 9 and 10, respectively. With a thick light guide, the value C_y is affected mainly by the v value at which $K_{yh}(v)$ is maximum, rather than by the light-guide thickness. Therefore, the request that $S_y(0,0) = S_y(0,\sqrt{3})$, may be met by a suitable adjustment of the y value mentioned above. This type of adjustment is relatively easy to realize by the delay-line position computation (*12–14*).

On the other hand, since C_x is only slightly affected

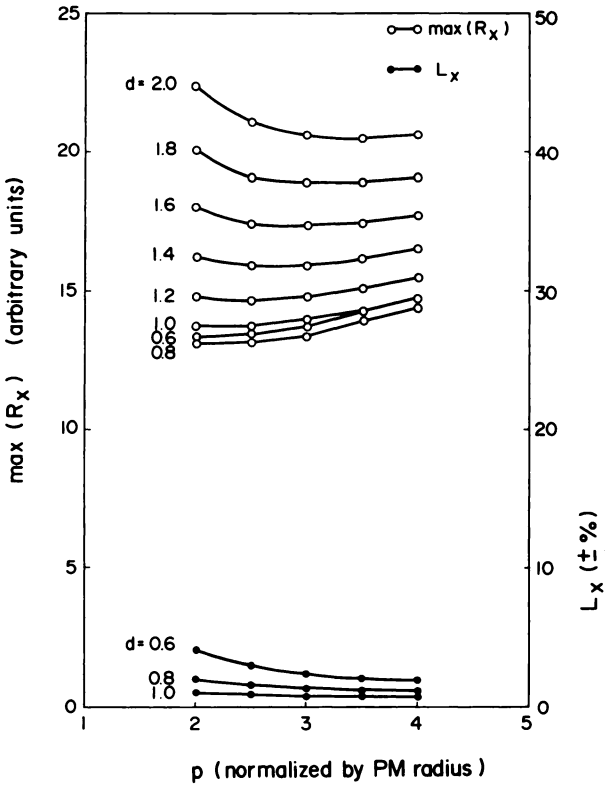

FIG. 11. Resolving distance and nonlinearity for x direction by $K_{xh}(u)$, obtained under same conditions as in Fig. 9.

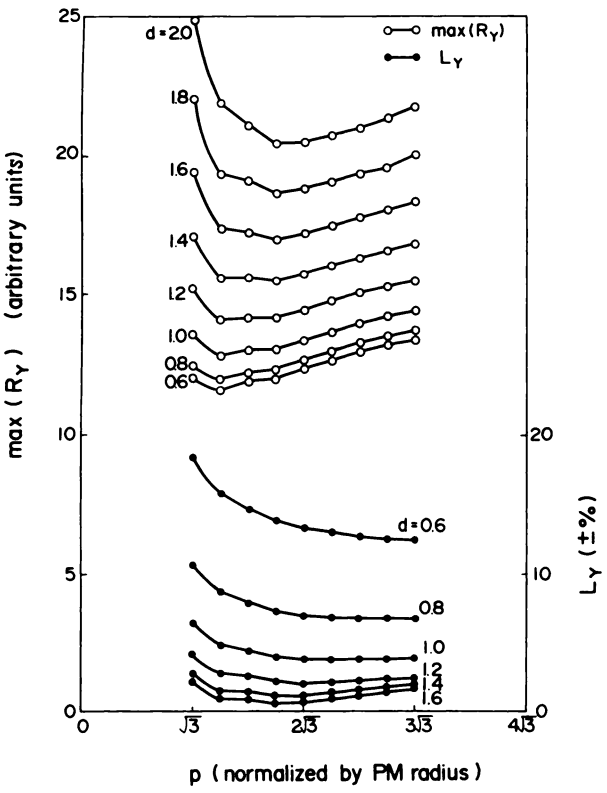

FIG. 12. Resolving distance and nonlinearity for y direction by $K_{yh}(v)$, obtained under same conditions as in Fig. 9.

by the u value at which $K_{xh}(u)$ is maximum, a large amount of $K_x(1)$ correction is required, in most cases, as the light-guide thickness decreases. When the light-guide is thin, the amount of correction required for $K_y(\sqrt{3}/2)$ is always less in comparison with $K_x(1)$, although C_y is also determined mainly by the light-guide thickness.

Critical adjustment of the contribution function should be made according to decreases in either the light-guide thickness or the values, u and v, that maximize $K_x(u)$ and $K_y(v)$, respectively (Fig. 9).

The nonlinearity and resolving distance attained by $K_{xh}(u)$ and $K_{yh}(v)$ were calculated over the xy plane. The results are shown in Figs. 11 and 12. The nonlinearity in the x direction appears to be markedly reduced compared with the value attained by the matrix method. The remaining nonlinearity results from the fact that $K_{xh}(u)$ is one-dimensional.

The nonlinearity in the y direction may be reduced to about half the value obtained by the matrix method. On the basis of Eq. 34, the main part of the remaining nonlinearity is inherent. From the comparison of Figs. 7 and 12, and Figs. 6 and 11, the nonlinearity is reduced and accompanied by no increase in $\max(R_y)$, and only by a slight increase in $\max(R_x)$. Although the resolution loss in the x direction increases as the light-guide thickness decreases, it remains within ±10% for d = 0.8.

DISCUSSION

For low-energy photons such as those emitted from Tc-99m (140 keV), the d value is roughly equivalent to the total optical thickness—the distance between the photocathode plane and the scintillation crystal surface where the photons enter—although the approximation cannot be applied to nonflat light guides. Typical d values have been 1.3 or more for the matrix or threshold-preamplifier methods (*10,24,25*). The limits of acceptable nonlinearity should be assumed to be ±4%, because Fig. 5 suggests that this value is realized for d = 1.3 by means of the matrix method. When d = 1.3, $\max(R_x)$ is 18.6 for the matrix method and 16.1 for the threshold-preamplifier method. The latter value can be obtained by interpolation in Fig. 6, in which the minimum value of $\max(R_x)$ is determined under the condition d = 1.3 and L_y = ±4%. Figure 12 suggests that d can be decreased to 1.0 by applying a corrected one-dimensional contribution function, when L_y is ±4%. According to Fig. 11, the minimum value of $\max(R_x)$ is 13.8 when d = 1.0. The improvement in $\max(R_x)$ attained by the d value decrease is 26% for the matrix method and 14% for the threshold-preamplifier method.

CONCLUSION

The statistical spatial resolution and coordinate linearity at the central portion of the image detector are investigated theoretically in relation to both the "contribution function" and "line-signal function." The concept of these functions permits evaluation of camera performance. Based on a simple light-distribution model for PM solid angles, results have been discussed for the "ideal," matrix, and threshold-preamplifier methods. In addition, modification of contribution functions, which reduce the coordinate nonlinearity, are presented.

The present work is the first study of the contribution function. Further analysis of a practical delay-line position-computation circuit will be reported in a separate paper. Some problems with regard to practical light distribution and edge-distortion compensation require investigation to clarify these areas more completely.

APPENDIX

1. Method for obtaining a solution for $h_x(u)$. Since $h_x(-u) = -h_x(u)$, and $-\partial N_x/\partial x(-u,v) = \partial N_x/\partial u(u,v)$, Eq. 24 can be rewritten as

$$S_{xh} = S_x(x_o,0) - h_x(x_o) \cdot \frac{\partial N_x}{\partial u}(x_o,0)$$

$$
\begin{aligned}
&- h_x(1 - x_o) \cdot \frac{\partial N_x}{\partial u}(1 - x_o, \sqrt{3}) \\
&- h_x(1 + x_o) \cdot \frac{\partial N_x}{\partial u}(1 + x_o, \sqrt{3}) \\
&- h_x(2 - x_o) \cdot \frac{\partial N_x}{\partial u}(2 - x_o, 0).
\end{aligned} \tag{39}
$$

Under the conditions in Eq. 25, the simultaneous equations can be obtained by the substitutions of $x_o = 0$ and $x_o = 1$ in Eq. 39. The values $h_x(1)$ and S_{xh} are obtained as the solutions of simultaneous equations, that is,

$$
h_x(1) = \frac{S_x(1,0) - S_x(0,0)}{2\left\{\frac{\partial N_x}{\partial u}(1,0) - \frac{\partial N_x}{\partial u}(1,\sqrt{3})\right\}} \tag{40}
$$

$$
S_{xh} = \frac{S_x(1,0)\frac{\partial N_x}{\partial u}(1,\sqrt{3}) - S_x(0,0)\frac{\partial N_x}{\partial u}(1,0)}{\frac{\partial N_x}{\partial u}(1,\sqrt{3}) - \frac{\partial N_x}{\partial u}(1,0)}. \tag{41}
$$

Equation 28 is derived from Eqs. 27 and 40.

If $h_x(u)$ is given at $1 \leqq |u| \leqq 2$, $h_x(x_o)$ and $h_x(1 - x_o)$ for a certain value of x_o may be obtained from the simultaneous equations, Eq. 39 and one obtained by substitution of $1 - x_o$ for x_o in Eq. 39. The procedure is applied repeatedly for each x_o in the range of $0 < x_o < 0.5$ to obtain the entire $h_x(u)$.

2. Derivation of Eq. 31. On the assumption that L_x may be approximated to

$$
L_x = \frac{S_x(1,0) - S_x(0,0)}{S_x(1,0) + S_x(0,0)} \cdot 100 \quad (\pm\%), \tag{42}
$$

a combination of Eqs. 23 and 42 leads to

$$
\begin{aligned}
\frac{\partial L}{\partial K_x(1)} &= 4\{S_x(1,0) \cdot \frac{\partial N_x}{\partial u}(1,\sqrt{3}) \\
&\quad - S_x(0,0) \cdot \frac{\partial N_x}{\partial u}(1,0)\} \\
&\quad \Big/ \{S_x(1,0) + S_x(0,0)\}^2.
\end{aligned} \tag{43}
$$

Therefore, we obtain

$$
\left.\frac{\partial L}{\partial K_x(1)}\right| K_x(1) = K_{xh}(1) = \frac{\frac{\partial N_x}{\partial u}(1,\sqrt{3}) - \frac{\partial N_x}{\partial u}(1,0)}{S_{xh}}. \tag{44}
$$

Equation 31 is derived from Eqs. 41 and 44.

3. Derivation of Eqs. 36 and 38. Expressions corresponding to Eqs. 23 and 39 are written as

$$
S_y(0,y_o) = -\sum K_y(v)\frac{\partial N_y}{\partial v}(u,v), \tag{45}
$$

and

$$
\begin{aligned}
S_{yh} &= S_y(0,y_o) - h_y(y_o) \cdot \frac{\partial N_y}{\partial v}(0,y_o) \\
&\quad - h_y(1 - y_o) \cdot \frac{\partial N_y}{\partial v}(1,1 - y_o),
\end{aligned} \tag{46}
$$

respectively. Equation 36 is derived from Eq. 46, since $S_{yh} = S_y(0,0)$ and $K_{yh}(v) = K_y(v) + h_y(v)$.

On the assumption that L_y may be approximated as

$$
L_y = \frac{S_y(0,\sqrt{3}/2) - S_y(0,0)}{S_y(0,\sqrt{3}/2) + S_y(0,0)} \cdot 100 \quad (\pm\%), \tag{47}
$$

we obtain the following from Eqs. 45 and 47:

$$
\begin{aligned}
&\frac{\partial L}{\partial K_y(\sqrt{3}/2)} \\
&\quad - S_y(0,\sqrt{3}/2) \cdot \\
&= \frac{\left\{\frac{\partial N_y}{\partial v}(0,\sqrt{3}/2) + \frac{\partial N_y}{\partial v}(1,\sqrt{3}/2)\right\}}{S_y(0,\sqrt{3}/2) + S_y(0,0)^2},
\end{aligned} \tag{48}
$$

and

$$
\left.\frac{\partial L}{\partial K_y(\sqrt{3}/2)}\right| K_y(\sqrt{3}/2) = K_{yh}(\sqrt{3}/2) = \frac{\frac{\partial N_y}{\partial v}(0,\sqrt{3}/2) + \frac{\partial N_y}{\partial v}(1,\sqrt{3}/2)}{-4 \cdot S_y(0,0)}. \tag{49}
$$

Equation 38 is derived from Eq. 49.

ACKNOWLEDGMENTS

The authors are indebted to Dr. Shinji Yamamoto and Dr. Teruichi Tomura of the Hitachi Central Research Laboratory for participating in valuable discussions and offering many useful suggestions.

A part of the present work was originally presented at the 37th Annual Meeting of the Japan Society of Applied Physics in October 1976.

REFERENCES

1. ANGER HO: Scintillation camera. *Rev Sci Instr* 29: 27–33, 1958
2. ANGER HO: Gamma-ray and positron scintillation camera. *Nucleonics* 21: No 10, 56–59, 1963
3. ANGER HO: Scintillation camera with multichannel collimators. *J Nucl Med* 5: 515–531, 1964
4. MALLARD JR, MYERS MJ: The performance of a gamma camera for the visualization of radioactive isotopes in vivo. *Phys Med Biol* 8: 165–182, 1963
5. CRADDUCK TD, GRAD IEE, FEDORUK SO: An experimental determination of the overall spatial resolution of a scintillation camera. *Phys Med Biol* 10: 67–76, 1965

6. MYERS MJ, KENNY PJ, LAUGHLIN JS, et al: Quantitative analysis of data from scintillation cameras. *Nucleonics* 24: No 2, 58–61, 1966

7. ANGER HO: Sensitivity, resolution, and linearity of the scintillation camera. *IEEE Trans* NS-13: 380–392, 1966

8. ANGER HO: Radioisotope cameras. In *Instrumentation in Nuclear Medicine*, Vol 1, Hine GJ, ed, New York, Academic Press, 1967, pp 485–552

9. BAKER RG, SCRIMGER JW: An investigation of the parameters in scintillation camera design. *Phys Med Biol* 12: 51–63, 1967

10. SVEDBERG JB: Image quality of a gamma camera system. *Phys Med Biol* 13: 597–610, 1968

11. TANAKA E, HIRAMOTO T, NOHARA N: Scintillation cameras based on new position arithmetics. *J Nucl Med* 11: 542–547, 1970

12. HIRAMOTO T, TANAKA E, NOHARA N: A scintillation camera based on delay-line time conversion. *J Nucl Med* 12: 160–165, 1971

13. NOHARA N, TANAKA E, HIRAMOTO T, et al: High-resolution scinticamera based on delay-line time conversion. *J Nucl Med* 12: 635–636, 1971

14. TANAKA E, NOHARA N, KUMANO N, et al: A large-area, high-resolution scintillation camera based on delay-line time conversion. In *Medical Radioisotopes Scintigraphy 1972*, Vol 1, Vienna, IAEA, 1973, pp 169–180

15. KULBERG GH, VAN DIJK N, MUEHLLEHNER G: Improved resolution of the Anger scintillation camera through the use of threshold preamplifiers. *J Nucl Med* 13: 169–171, 1972

16. TAKAMI K, UEDA K, KAWAGUCHI F, et al: Optical character of scintillators of scintillation camera. *Preliminary Reports for the 37th Annual Meeting of the Japan Society of Applied Physics*: 104, 1976

17. UEDA K, TOMURA T, YAMAMOTO S, et al: Analysis of optical systems of scintillation camera. *Preliminary Reports for the 37th Annual Meeting of the Japan Society of Applied Physics*: 105, 1976

18. KAWAGUCHI F, UEDA K, TAKAMI K, et al: A position computation for scintillation cameras based on delay-line time conversion. *Preliminary Reports for the 37th Annual Meeting of the Japan Society of Applied Physics*: 106, 1976

19. SHIONO H, SUZUKI R, KOHNO H, et al: A position computation for scintillation cameras based on function generating method. *Preliminary Reports for the 37th Annual Meeting of the Japan Society of Applied Physics*: 107, 1976

20. UEDA K, KAWAGUCHI F, TAKAMI K, et al: Performance of a newly developed scintillation camera. *Preliminary Reports for the 37th Annual Meeting of the Japan Society of Applied Physics*: 108, 1976

21. SCRIMGER JW, BAKER RG: Investigation of light distribution from scintillations in a gamma camera crystal. *Phys Med Biol* 12: 101–103, 1967

22. MASKET AVH, RODGERS WC: Tables of solid angles. *USAEC Report* TID-14975: 1–16, 1962

23. KULBERG GH, MUEHLLEHNER G: Scintillation camera with improved resolution. *US Patent* 3,732,419, 1971

24. MARTONE RJ, GOLDMAN SC, HEATON CC: Scintillation camera with light diffusion system. *US Patent* 3,784,819, 1971

25. MUEHLLEHNER G: Radiation imaging device. *US Patent* 3,745,345, 1971